

Antireflection Coating for MWIR on Calcium Fluoride Using Ion-Assisted E-Beam Deposition

Yusuf Dogan^{1,2} , İlhan Erdogan^{1,2*} 

¹ Department of Electrical and Electronics Engineering, Sivas University of Science and Technology, Sivas, Türkiye

² Optical Excellence Application and Research Center, Sivas University of Science and Technology, Sivas, Türkiye

* ilhan.erdogan@sivas.edu.tr

* Orcid No: 0000-0002-2774-1349

Received: July 28, 2024

Accepted: March 3, 2025

DOI: 10.18466/cbayarfbe.1523797

Abstract

This research outlines the design, analysis, and fabrication of a multilayer anti-reflective coating on a calcium fluoride (CaF₂) substrate, specifically for mid-wavelength infrared uses, employing the ion-assisted electron-beam evaporation method. A 2-layered multilayer structure in the form of SiO₂/Ge was created on CaF₂, consisting of low refractive index silicon dioxide (SiO₂) and high refractive index germanium (Ge) thin films with a total thickness below 1 µm. The design was optimized for the 3.6-4.9 µm MWIR range, and an average transmission of 98.39% and an average reflectance of 0.93% were simulated at a broadband spectral width of 1300 nm. After the fabrication process using the ion-assisted physical vapour deposition (IAPVD) technique, the experimental results showed an average transmission of 98.13% and a reflectance value of 1.19% within the 3.6-4.9 µm range. The simulation design and experimental results were found to be very close to each other, with a difference of only 0.26%. This work provides a high-efficiency solution for AR coatings in the MWIR region on CaF₂ surfaces. To our knowledge, the Ge/SiO₂ multilayer structure on CaF₂ has not been reported before in the literature and the results obtained will be an alternative for CaF₂-based optical systems.

Keywords: Mid-wave infrared (MWIR), Calcium fluoride, Optical thin films, Anti-reflective coating, Ion-assisted e-beam deposition

1. Introduction

Antireflective (AR) coatings are thin films applied to optical components to minimize reflections and maximize light transmission. These coatings are essential and indispensable in various fields due to their broad range of applications, from infrared sensors to everyday eyeglasses. By reducing reflections, AR coatings enhance the transmission of light through optical elements, improving sensitivity, accuracy, and overall system performance [1]. In solar panels, AR coatings enhance energy efficiency by allowing more sunlight to be absorbed and converted into electricity. On eyeglasses, AR coatings reduce glare and reflections, improving visual clarity and comfort. For camera lenses, they minimize reflections and lens flare, resulting in sharper, higher-quality photographs. On display screens like those on smartphones and monitors, AR coatings reduce ambient light glare, improving visibility and user experience. In microscopes, AR coatings improve light

transmission and image contrast, enabling clearer and more detailed observations in scientific research [2-5]. AR coatings are particularly important for applications involving infrared radiation, which covers wavelengths longer than visible light but shorter than microwaves. Mid-wavelength infrared (MWIR) range (3-5 µm) being particularly important for applications such as thermal imaging, night vision, space, and environmental monitoring [6, 7]. In electro-optical systems, AR coatings increase light transmission through optical elements, enhance image quality, and improve overall system performance by minimizing signal loss and glare. This enhancement is critical for detecting temperature differences in thermal imaging and other similar applications.

The multilayer structure of AR coatings is essential for achieving optimal performance, as each layer is designed to target specific wavelengths, further reducing reflections and enhancing light transmission across a broad spectrum [8]. These coatings are designed to

minimize reflectance within this specific range by carefully selecting materials and controlling each layer's thickness and refractive index. Germanium (Ge) and silicon dioxide (SiO₂) are crucial optical materials in this range due to their effective AR properties and common use in infrared thin films. SiO₂, with a low refractive index of 1.44 at 4 μm, is favored for its availability, chemical stability, high-temperature resistance, cost-effectiveness, low dispersion, eco-friendliness, excellent adhesion to various surfaces, and good transmission in both visible and infrared ranges, along with notable scratch resistance [9, 10]. Meanwhile, Ge, a high-index material with a refractive index of 4.0 at 4 μm, offers benefits such as insolubility, effective transmission, chemical inertness, low dispersion, non-toxicity, good thermal conductivity, and durability within the infrared range [7, 11, 12]. Calcium fluoride (CaF₂) is an ideal substrate for optical thin films due to its excellent optical properties and chemical stability. It has a wide transmission range from deep ultraviolet (UV) to infrared (IR), making it suitable for diverse optical applications [13, 14]. CaF₂'s low refractive index minimizes reflection losses, which is beneficial in multi-layer coatings for maintaining high transmittance. It also has a high laser damage threshold, making it suitable for high-power laser applications. Its low solubility in water and resistance to chemical attack ensure the durability and longevity of optical components. These properties make CaF₂ a preferred substrate for spectroscopy, lithography, and other advanced optical systems. Moreover, its transparency range, low refractive index, chemical stability, and resistance to moisture make it advantageous for AR coatings, offering a non-toxic and durable solution for precision optical components [15, 16].

AR thin films can be produced through various methods including physical vapor deposition (PVD), chemical vapor deposition (CVD), magnetron sputtering, and the sol-gel process [4, 17-19]. The ion-assisted electron-beam (e-beam) deposition technique provides better control, higher film quality, reduced contamination, and greater process flexibility compared to traditional e-beam evaporation methods. In this study, an ion-assisted e-beam PVD technique was employed for the experiment. So far, numerous studies have fabricated and developed high-performance AR coatings in the MWIR spectrum range using the e-beam PVD technique. Various multilayer stacks have been implemented on different substrates such as Si [6, 7, 9, 20, 21], Ge [7, 22, 23], ZnS [24], and ZnSe [25]. Studies in the literature mainly focused on Si and Ge substrates for the MWIR region. However, the literature on CaF₂ substrates is limited, and among the studies conducted in the MWIR region with CaF₂ substrates, one focuses on a ZnS/YbF₃/Y₂O₃ 5-layer multilayer stack, presented [26] as a conference proceeding. In addition, Yenisooy et al. [27] proposed a multilayer stack of aluminum oxide (Al₂O₃) and Ge on a CaF₂ substrate. In this study, we proposed a Ge/SiO₂

multilayer stack on a CaF₂ substrate which has not been presented in the literature before.

This research details the development and manufacture of a wideband AR multilayer coating intended for CaF₂ optics, specifically targeting the MWIR spectrum. The coating was created using ion-assisted e-beam physical vapor deposition. Before the fabrication, OptiLayer software is used to design and optimize the SiO₂/Ge/CaF₂ Substrate/Ge/SiO₂ multilayer structure, and average transmission (T_{av}) of 98.39% and an average reflection (R_{av}) of 0.93% values are simulated. After the e-beam evaporation process, an average transmission (T_{av}) of 98.13% and an average reflection (R_{av}) of 1.19% is achieved through the double-sided coated structure. The study demonstrates superior transmission performance on CaF₂ optics within the 3.6-4.9 μm MWIR range, marking it as a noteworthy advancement. Moreover, the proposed AR multilayer structure is noted for its cost-effectiveness, attributed to its overall thickness and layer count.

2. Materials and Methods

Multilayer thin film coatings are essential in AR coatings because they can manipulate light precisely, enhancing the performance of optical systems by improving reflection, and transmission as needed. In these coatings, the desired transmission or reflection characteristics are achieved by optimizing the thickness of layers with high and low refractive indices. Compared to single-layer coatings, multilayer structures offer better control, a broader wavelength range, and superior performance, making them more suitable for complex applications such as narrow-band filters, high-performance mirrors, and dual/triple-band structures [1, 5]. Coating materials are chosen based on their refractive index, physical stability, transparency in the targeted wavelength regions, and thermal expansion coefficients. A multilayer stack of optical thin film coatings, comprising alternating layers of materials with different refractive indices, is deposited on a substrate. The thickness of each layer is precisely controlled to the nanometer scale to regulate light transmission and reflection through constructive and destructive interference. The multilayer design was simulated using OptiLayer software which is a specialized software suite essential for designing, analyzing, and optimizing optical coatings. It enables the creation and simulation of complex multilayer structures, using advanced algorithms and a comprehensive material database to achieve desired optical properties efficiently. The software provides detailed spectral analysis and simulates performance at different angles of incidence. It supports manufacturing processes by assessing production tolerances, enabling reverse engineering, and integrating with deposition equipment for real-time monitoring. The target design consists of 100% transmittance and 0% reflectance values distributed over 126 linearly spaced spectral points at a 0° incident angle

in the 3.6-4.9 μm wavelength range. Target interpolation was performed to align the desired spectral characteristics with the material design parameters. To achieve this, an optimization method was selected, employing the Modified Damped Least Squares (Modified DLS) algorithm. This method is particularly effective, offering rapid convergence during the initial stages of the refinement process. The Modified DLS algorithm remains a robust choice for refining intricate optical designs with high precision. The termination criteria for the Gradual Evolution setup are defined to ensure an optimized design process. The merit function is set to a threshold value of 0.5, which serves as a key indicator of convergence during the optimization.

The designed Ge/SiO₂ thin film stacks on both sides of the CaF₂ substrate have been implemented, as shown in Figure 1. In this multilayer stack, SiO₂ and Ge are used as the low (nL) and high (nH) refractive index materials, respectively. AR coatings are designed to ensure a 180° relative phase shift between the beams reflected at the top and bottom surfaces of a thin film. This results in destructive interference, which cancels out both reflected beams. The optical thickness of the coating must be an odd multiple of $\lambda/4$, where λ represents the design wavelength. This configuration is essential to create a path difference of $\lambda/2$ between the reflected beams, leading to their cancellation. The refractive index of the thin film required to achieve complete beam cancellation can be calculated using the refractive indices of the incident medium and the substrate. In the design of AR coatings, the fundamental principle for single-layer films relies on the refractive index matching between the coating material, the incident medium, and the substrate. This relationship is described by the following equation:

$$n_{film} = \sqrt{n_{medium} \cdot n_{substrate}} \quad (1)$$

For single-layer thin films, optimal antireflection is achieved when the optical thickness corresponds to a quarter wavelength of light. In contrast, for multilayer coatings, the layers are typically arranged to have optical thicknesses of either quarter-wavelength or half-wavelength according to their refractive index values. Multilayer structures are designed to provide enhanced reflection control over a broader spectral range and to achieve the desired optical performance. This design approach requires careful optimization of both the refractive index and the thickness of each layer.

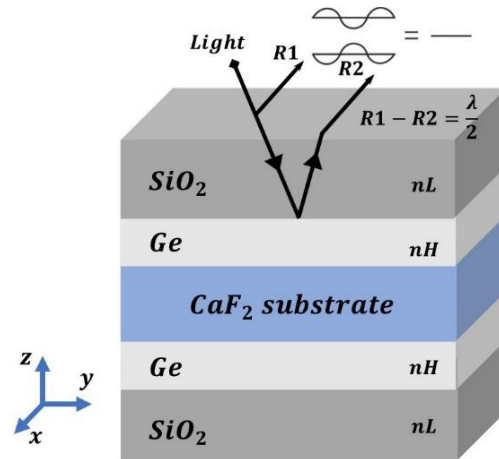


Figure 1. Schematic representation of double-sided multilayer structure

Due to its high melting and boiling points, low thermal expansion coefficient, substantial hardness, and excellent mechanical stability, CaF₂ is an ideal material for various optical applications, ensuring durability and reliability in demanding environments. The technical specifications of CaF₂ are provided in Table 1.

Table 1. Technical specifications of the CaF₂ substrate

Property	Value	Unit	Ref.
Transmission Range	0.3-11	-	[28]
Refractive Index	1.3-1.48	-	[29]
Density	3.18	g/cm ³	[30]
Melting Point	1418	C°	[31]
Boiling Point	2533	C°	[32]
Laser damage threshold	10	J/cm ²	[33]
Thermal Expansion Coefficient	18.85	1/ C°	[30]
	x10 ⁻⁶		
Knoop's hardness, HK ₃₀₀	152-159	kg/mm ²	[30]
Young's modulus	75.8	GPa	[34]
Abbe number	95.13	-	[29]

The Hartmann dispersion equation is a mathematical representation used to describe the wavelength-dependent refractive index of optical materials [35]. This equation, often applied in the field of optics, allows for the precise characterization of materials by relating the refractive index to the wavelength of light passing through the material. The equation typically includes parameters that account for the material's intrinsic properties, such as dispersion coefficients. The dispersion formula is an empirical relationship used to describe how the refractive index of Ge and SiO₂ thin films and CaF₂ substrate varies with wavelength. The equation is given by

$$n(\lambda) = A_0 + \frac{A_1}{\lambda - A_2} \quad (2)$$

where $n(\lambda)$ is the refractive index at wavelength λ , A_0 , A_1 and A_2 are coefficients specific to the material. The Hartmann constants for a 1 mm thick CaF_2 substrate are found as 0.10, 187.98, and -139.6, for A_0 , A_1 , and A_2 , respectively. The values for the constants in the Hartmann dispersion equation were obtained by fitting experimental transmission measurements of the CaF_2 substrate. The experimental and modeled transmission and reflection spectra for a CaF_2 substrate over the MWIR range are shown in Figure 2 (a) and (b). These data exhibit a strong correlation, indicating that the theoretical model accurately represents the observed transmission and reflection spectra for the CaF_2 substrate in the MWIR range. The measurements were taken using a PerkinElmer FT-IR (Fourier-transform infrared spectroscopy) device.

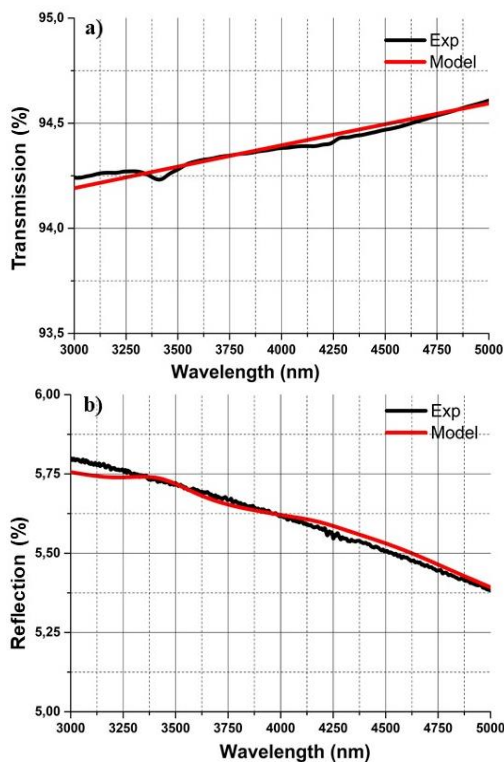


Figure 2. Experimental and modeled transmission and reflection spectra for CaF_2 substrate

Before initiating the multilayer design process, it is crucial to analyze the optical properties of individual layers comprehensively. Such evaluations are indispensable for understanding and optimizing the interactions between the layers in a multilayer structure. Each layer may be composed of distinct optical materials, each contributing uniquely to the overall optical performance. By examining these properties independently, designers can ensure proper refractive

index matching, thickness control, and spectral behavior, which are critical for achieving the desired functionality in the final multilayer configuration. To accurately simulate the refractive index dispersions in thin films, a 300 nm thick Ge film on a CaF_2 substrate and a 400 nm thick SiO_2 film on a Ge substrate are coated via e-beam evaporation. Figure 3 (a) depicts the transmission curves of 300 nm Ge and 400 nm SiO_2 thin films. The dispersion coefficients for the Ge film and SiO_2 film were determined as $A_0=4.258$, $A_1=0.003$, and $A_2=2.78$. and $A_0=0.1$, $A_1=75.64$, and $A_2=-51.73$, respectively. The dispersion coefficients A_0 , A_1 , and A_2 were calculated by fitting experimental transmission measurements of Ge and SiO_2 coated substrates. These coefficients facilitate the prediction of refractive indices across different wavelengths, enabling the customization and enhancement of optical thin film coatings with specific desired characteristics. The refractive index dispersions of Ge and SiO_2 thin films and CaF_2 substrate are illustrated in Figure 3 (b).

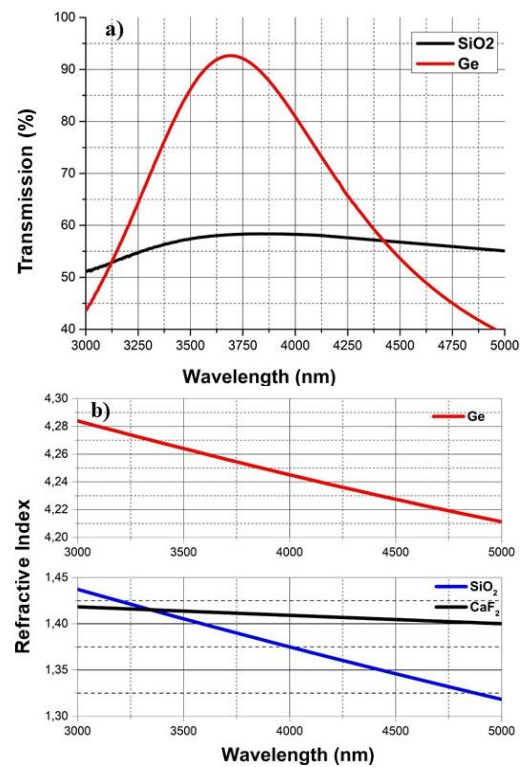


Figure 3. a) Transmission spectra of SiO_2 and Ge b) Refractive index dispersions of Ge film, SiO_2 film, and CaF_2 substrate

Refractive index distribution models were defined for the substrate and layer materials, and the multilayer AR coating design for the wavelength range of 3.6 to 4.9 μm was obtained using the Optilayer software. Thanks to gradual and needle optimizations, the optimized design reached R_{av} and T_{av} values of 0.93% and 98.39%, respectively. The optimized total thickness of the multilayer stack is approximately 889.79 nm. The quarter wavelength optical thickness (QWOT) of the layer

materials was defined for a control wavelength of 4 μm . The refractive indices of Ge, SiO₂, and CaF₂ at a center wavelength of 4 μm are found to be 4.245, 1.375, and 1.41, respectively. Table 2 shows the materials RI and layer thicknesses of the designed multilayer structure.

Table 2. Optical parameters of the designed multilayer AR coating

Material	Optical		
	Thickness (nm)	QWOT	RI at 4 μm
SiO ₂	852,787	1,193	1.375
Ge	37,003	0,148	4.245
CaF ₂	1 (mm)		1.41

The deposition of the thin films was carried out using the e-beam evaporation technique, with an ion plasma source. The e-beam PVD system used in this study is equipped with a dual electron beam configuration, consisting of a continuous single-pocket system and a six-pocket crucible system, enabling the deposition of various materials without interrupting the process for material changes. By combining the vaporized coating material with ion bombardment, the system enhances the density and adhesion of the thin film, resulting in a higher quality and more durable coating. To generate the ion plasma necessary for the deposition process, Argon (Ar) gas was introduced into the vacuum chamber. The use of argon facilitates the creation of a stable plasma, which is critical for the effective evaporation and deposition of the thin films to improve the adhesion and quality of the coating. The chamber's temperature was controlled and maintained uniformly using halogen heaters, ensuring a stable thermal environment essential for high-quality film growth. To monitor and control the deposition rate and the thickness of the deposited layers, a 6 MHz gold piezoelectric Quartz Crystal Microbalance (QCM) was employed. Figure 4 illustrates the inner chamber of the ion-assisted electron beam deposition system used in this study, showcasing its advanced design and functional versatility tailored for thin film fabrication.

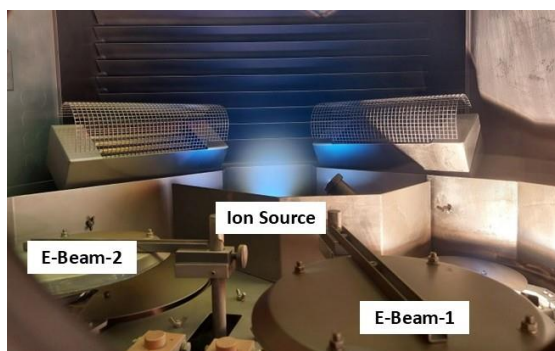


Figure 4: Inner chamber of ion-assisted E-beam PVD system

By optimizing the deposition conditions, including the ion plasma generation, temperature regulation, and real-time monitoring, high-quality Ge and SiO₂ thin films with refractive index distributions were successfully fabricated. Optical analysis is conducted to assess the coating's transmission, reflection, and surface quality. Upon detecting deviations from the expected outputs, an optimization process is commenced by modifying deposition parameters such as gas flow rates, deposition rates, temperature, ion parameters, and e-gun parameters. This iterative procedure guarantees an AR coating with desired optical characteristics. The flow chart of the AR coating process is depicted in Figure 5.

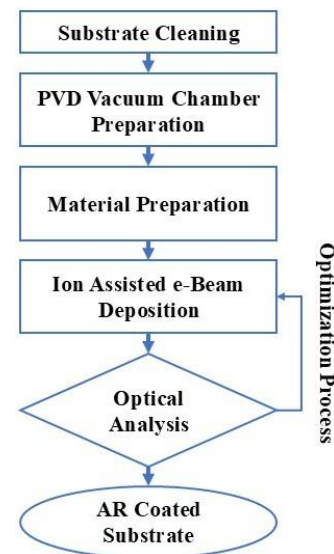


Figure 5: Flow chart of the PVD deposition process

Before deposition, the 1-inch CaF₂ substrate underwent a precleaning process to remove native oxide and contaminants, involving a rinse with acetone followed by nitrogen gas drying. During deposition, the base vacuum level was maintained at 2×10^{-7} Torr, while the process vacuum level was controlled at about 2×10^{-4} Torr, and the chamber temperature was kept at 200 °C. High-purity Ge (99.999%) and SiO₂ (99.99%) granules were placed into the crucible in the water-cooled hearth. The vaporization sequence for SiO₂ and Ge materials was followed precisely, with deposition rates of 1 nm/s for both. To ensure uniform coating, the sample holder was continuously rotated at 20 rpm. During SiO₂ vaporization, oxygen gas was introduced into the PVD chamber at a flow rate of 10 sccm, which was critical for maintaining the purity and quality of the SiO₂ layer. The optical properties of the coated multilayer AR coatings were evaluated using an FT-IR spectrometer to measure transmission and reflectance at a 10° incidence angle. Additionally, the surface roughness of the coated multilayer AR coatings was assessed using a Profilm 3D white light interferometry (WLI) profiler equipped with a 20x Michelson objective.

3. Results and Discussion

The CaF₂ substrate surfaces were thoroughly cleaned using deionized water and acetone, and then dried with nitrogen to remove any dust or natural oxides. After cleaning, a white light interferometer (Filmetrics, 3D) was used to assess how deposition affected the surface quality of the samples. Figure 6 illustrates the surface roughness profiles of the CaF₂ substrate before (a) and after (b) applying multiple layers, with a scan area of 1x1 mm. The surface roughness (Sq) values were measured as 3.04 nm (standard deviation 0.17) for the uncoated surface and 2.45 nm (standard deviation 0.07) for the coated surface.

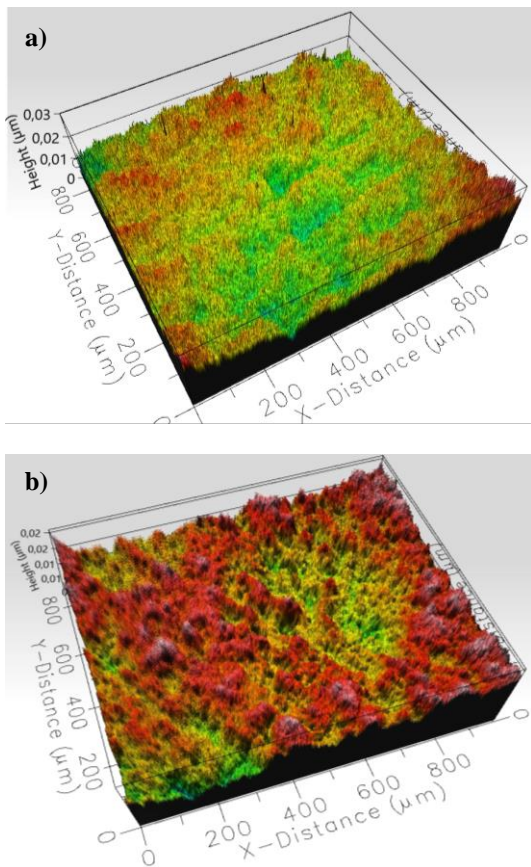


Figure 6. Surface profiles of CaF₂ substrate a) before and b) after multilayer deposition

Following the predefined process parameters, a multi-stack of SiO₂ and Ge materials was coated onto a CaF₂ substrate. Identical layer sequences and process conditions were applied to both sides of the CaF₂ substrate to reduce reflections from the rear surface. Figure 7 displays the transmission and reflection spectra of the double-side multilayer (SiO₂/Ge/CaF₂ Substrate/Ge/SiO₂) AR coating within the 3-5 μm MWIR range. Figure 7 (a) shows that the simulated transmission spectrum closely matches the measured transmission, indicating a good correlation. Minor deviations can be attributed to variations in material thickness and inherent

absorbance properties, which affect the optical path length and cause energy loss at specific wavelengths, leading to the observed discrepancies. In the 3.6-4.9 μm MWIR range, the average transmission (T) is 98.39% for the simulated data and 98.13% for the measured data. The peak transmission values are 98.98% at 4196 nm for the measured data and 99% at 3983 nm for the simulated data. Similarly, as shown in Figure 7 (b), the simulated reflection spectrum closely aligns with the measured reflection, demonstrating a strong agreement. In the 3.6-4.9 μm MWIR range, the average reflection (Rav) is 0.93% for the simulated data and 1.19% for the measured data. The minimum reflection values are 0.1% at 4120 nm for the simulated data and 0.46% at 4112 nm for the measured data.

Additionally, the inherent absorbance properties of the materials, which can cause energy loss at specific wavelengths, contribute to the observed deviations. These factors highlight the sensitivity of the spectra to physical and material parameters, emphasizing the importance of precise control and characterization in experimental setups. Moreover, the discrepancy in measured reflection values compared to the simulated data is due to the difference in incident angles between the design (AOI=0°) and the FTIR measurement (AOI=10°). Table 3 presents the Rav and Tav values of the simulated and measured curves.

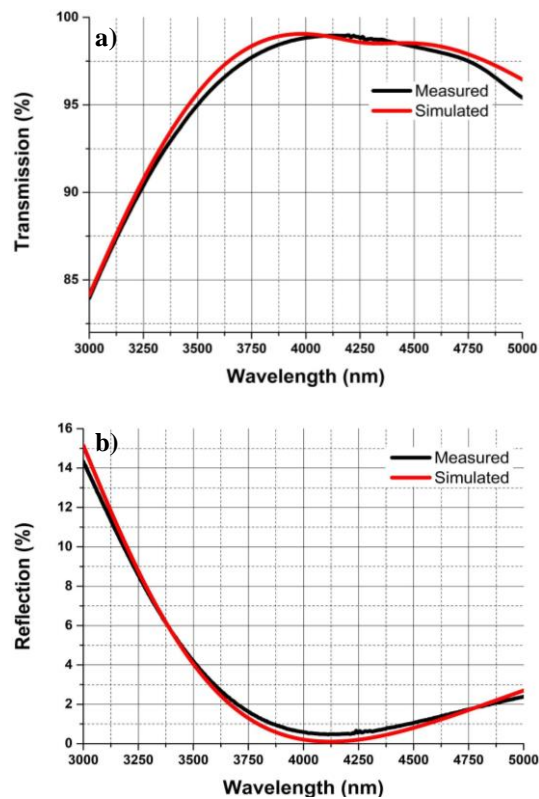


Figure 7. Measured and simulated spectra of the double-side multilayer (SiO₂/Ge/CaF₂ Substrate/Ge/SiO₂) AR coating a) Transmission b) Reflection

Table 3. Simulated and measured values of the double side multilayer (SiO₂/Ge/CaF₂ Substrate/Ge/SiO₂) AR coating for Tav and Rav in 3.6-4.9 μm.

Parameters	Simulated %	Real %
Tav	98.39	98.13
Rav	0.93	1.19

4. Conclusion

This study successfully demonstrated the design and fabrication of a highly efficient broad-band multilayer AR coating on a CaF₂ substrate, targeting the 3.6-4.9 μm wavelengths of the MWIR spectrum. The coating was applied using the ion-assisted e-beam evaporation technique, ensuring precise layer deposition and optimal optical performance. The experimental results showed a close match between the simulated and measured transmission and reflection spectra, with minor deviations attributed to thickness variations and absorbance effects. In the 3.6-4.9 μm range, the average transmission (Tav) was 98.39% for simulations 98.13% for measured data, while the average reflection (Rav) was 0.93% and 1.19%, respectively. Additionally, this study is particularly significant due to the shortage of multilayer AR coating research on CaF₂ substrates. The successful implementation of this bi-layer (SiO₂/Ge/CaF₂ Substrate/Ge/SiO₂) AR multilayer structure on a CaF₂ substrate marks a significant advancement, offering an effective coating solution for high-performance CaF₂-based optical components in MWIR electro-optical applications. Our study emphasizes the use of SiO₂, an eco-friendly, chemically stable material, combined with Ge in a simplified bilayer design, providing a cost-effective, highly applicable, easy-to-replicate, and innovative MWIR AR coating compared with the more resource-intensive other designs. Moreover, the reduced number of layers and thinner total thickness in our study make the production process significantly easier and more efficient compared to the thicker, 5-layer structures, which are inherently more complex and challenging to manufacture. The findings from this study contribute to the ongoing development of advanced AR coating designs, setting the stage for future research to explore new materials, deposition techniques, and innovative designs to further enhance AR coating technology in the MWIR region.

Author's Contributions

Yusuf Dogan: Supervision, Writing – review & editing, Writing – original draft, Methodology

İlhan Erdogan: Writing – review & editing, Writing – original draft, Software.

Ethics

There are no ethical issues after the publication of this manuscript.

References

- [1]. Raut, H. K., Ganesh, V. A., Nair, A. S., Ramakrishna, S. 2011. Anti-reflective coatings: A critical, in-depth review. *Energy & Environmental Science*; 4(10): 3779-3804. doi: 10.1039/C1EE01297E.
- [2]. Ji, C., et al. Recent Applications of Antireflection Coatings in Solar Cells. *Photonics*; 9(12). doi: 10.3390/photonics9120906.
- [3]. Bouhafs, D., Moussi, A., Chikouche, A., Ruiz, J. M. 1998. Design and simulation of antireflection coating systems for optoelectronic devices: Application to silicon solar cells. *Solar Energy Materials and Solar Cells*; 52(1): 79-93. doi: 10.1016/S0927-0248(97)00273-0.
- [4]. Chen, D. 2001. Anti-reflection (AR) coatings made by sol-gel processes: A review. *Solar Energy Materials and Solar Cells*; 68(3): 313-336. doi: 10.1016/S0927-0248(00)00365-2.
- [5]. Kaminski, P. M., Lisco, F., Walls, J. M. 2014. Multilayer Broadband Antireflective Coatings for More Efficient Thin Film CdTe Solar Cells. *IEEE Journal of Photovoltaics*; 4(1): 452-456. doi: 10.1109/JPHOTOV.2013.2284064.
- [6]. Yeniso, A., Yeşilyaprak, C., Tüzemen, S. 2019. High efficient ultra-broadband anti-reflection coating on silicon for infrared applications. *Infrared Physics & Technology*; 100: 82-86. doi: 10.1016/j.infrared.2019.05.014.
- [7]. Bhatt, M., Nautiyal, B. B., Bandyopadhyay, P. K. 2010. High efficiency antireflection coating in MWIR region (3.6–4.9 μm) simultaneously effective for Germanium and Silicon optics. *Infrared Physics & Technology*; 53(1): 33-36. doi: 10.1016/j.infrared.2009.08.006.
- [8]. Valiei, M., Shaibani, P. M., Abdizadeh, H., Kolahdouz, M., Asl Soleimani, E., Poursafar, J. 2022. Design and optimization of single, double and multilayer anti-reflection coatings on planar and textured surface of silicon solar cells. *Materials Today Communications*; 32: 104144. doi: 10.1016/j.mtcomm.2022.104144.
- [9]. Kala, M. B., Bandyopadhyay, P. K., Nautiyal, B. B. 2012. Thorium free antireflection coating in MWIR region on Silicon optics. *Infrared Physics & Technology*; 55(5): 409-411. doi: 10.1016/j.infrared.2012.05.005.
- [10]. Amirzada, M. R., Khan, Y., Ehsan, M. K., Rehman, A. U., Jamali, A. A., Khatri, A. R. Prediction of Surface Roughness as a Function of Temperature for SiO₂ Thin-Film in PECVD Process. *Micromachines*; 13(2). doi: 10.3390/mi13020314.
- [11]. Melcher, F., Buchholz, P. 2014. Germanium. In: Gunn, A. G. (ed.) *Critical Metals Handbook*; Wiley, pp. 177-203.
- [12]. Harris, D. C. 1999. *Materials for Infrared Windows and Domes: Properties and Performance*. SPIE Press.
- [13]. Thomas, I. M. 1988. Porous fluoride antireflective coatings. *Applied Optics*; 27(16): 3356-3358. doi: 10.1364/AO.27.003356.
- [14]. Deng, C.-Z., et al. 2019. Two-pair multilayer Bloch surface wave platform in the near- and mid-infrared regions. *Applied Physics Letters*; 115(9): 091102. doi: 10.1063/1.5101008.
- [15]. Yan, J., Syoji, K., Tamaki, J. I. 2003. Crystallographic effects in micro/nanomachining of single-crystal calcium fluoride. *Journal of Vacuum Science & Technology B: Microelectronics and Nanometer Structures Processing, Measurement, and Phenomena*; 22(1): 46-51. doi: 10.1116/1.1633770.

- [16]. Çetin, N. E., et al. 2013. The structural, optical and morphological properties of CaF₂ thin films by using Thermionic Vacuum Arc (TVA). *Materials Letters*; 91: 175-178. doi: 10.1016/j.matlet.2012.07.086.
- [17]. Zambrano, D. F., et al. 2021. Mechanical and microstructural properties of broadband anti-reflective TiO₂/SiO₂ coatings for photovoltaic applications fabricated by magnetron sputtering. *Solar Energy Materials and Solar Cells*; 220: 110841. doi: 10.1016/j.solmat.2020.110841.
- [18]. Varade, A., Krishna, A., Reddy, K. N., Chellamalai, M., Shashikumar, P. V. 2014. Diamond-like Carbon Coating Made by RF Plasma Enhanced Chemical Vapour Deposition for Protective Antireflective Coatings on Germanium. *Procedia Materials Science*; 5: 1015-1019. doi: 10.1016/j.mspro.2014.07.390.
- [19]. Choi, W. S., Kim, K., Yi, J., Hong, B. 2008. Diamond-like carbon protective anti-reflection coating for Si solar cell. *Materials Letters*; 62(4): 577-580. doi: 10.1016/j.matlet.2007.06.019.
- [20]. Duris, M., Deubel, D., Bodiou, L., Vaudry, C., Keromnes, J. C., Charrier, J. 2021. Fabrication of Ge-ZnS multilayered optical filters for mid-infrared applications. *Thin Solid Films*; 719: 138488. doi: 10.1016/j.tsf.2020.138488.
- [21]. Zhu, Z., et al. 2023. Scratch-resistant antireflective coating for mid-wave infrared band. *Infrared Physics & Technology*; 133: 104807. doi: 10.1016/j.infrared.2023.104807.
- [22]. Yenisoy, A., Yesilyaprak, C., Ruzgar, K., Tuzemen, S. 2019. Ultra-broad band antireflection coating at mid wave infrared for high efficient germanium optics. *Optical Materials Express*; 9(7): 3123-3131. doi: 10.1364/OME.9.003123.
- [23]. Dogan, Y., Erdogan, İ., Altuntepe, A. 2024. Design and fabrication of highly efficient antireflective coating in MWIR on germanium using ion-assisted e-beam deposition. *Optical Materials*; 157: 116362. doi: 10.1016/j.optmat.2024.116362.
- [24]. Awasthi, S., Nautiyal, B. B., Kumar, R., Bandyopadhyay, P. K. 2012. Multi-spectral antireflection coating on zinc sulphide simultaneously effective in visible, eye safe laser wavelength and MWIR region. *Infrared Physics & Technology*; 55(5): 395-398. doi: 10.1016/j.infrared.2012.06.003.
- [25]. Lemarquis, F., Marchand, G., Amra, C. 1998. Design and manufacture of low-absorption ZnS-YF₃ antireflection coatings in the 3.5–16- μ m spectral range. *Applied Optics*; 37(19): 4239-4244. doi: 10.1364/AO.37.004239.
- [26]. Yao-ping, Z., Jun-qi, F., Hong, X. 2012. Anti-reflection coating on calcium fluoride substrate using ion-assisted deposition. In: *Proceedings of SPIE*; 8416: 84161Q. doi: 10.1117/12.976048.
- [27]. Yenisoy, A., Tüzemen, S. 2020. Development of high efficient and ultra-broadband antireflection coating on calcium fluoride for electro-optical applications. *Surface Engineering*; 36(4): 364-370. doi: 10.1080/02670844.2019.1644936.
- [28]. Michael, E. C. 2001. Challenges in IR optics. In: *Proceedings of SPIE*; 4369: 649-661. doi: 10.1117/12.445327.
- [29]. Malitson, I. H. 1963. A Redetermination of Some Optical Properties of Calcium Fluoride. *Applied Optics*; 2(11): 1103-1107. doi: 10.1364/AO.2.001103.
- [30]. Retherford, R. S., Sabia, R., Sokira, V. P. 2001. Effect of surface quality on transmission performance for (111) CaF₂. *Applied Surface Science*; 183(3): 264-269. doi: 10.1016/S0169-4332(01)00587-6.
- [31]. Jacob, R., Sergeev, D., Yazhenskikh, E., Müller, M. 2023. Evaluation of the calcium chloride-calcium fluoride system for high temperature thermal energy storage. *Journal of Energy Storage*; 72: 108521. doi: 10.1016/j.est.2023.108521.
- [32]. Choi, J. H., Na, H., Park, J., Kim, H.-J. 2019. Plasma corrosion resistance of aluminosilicate glasses containing Ca, Y and B under fluorocarbon plasma with Ar+. *Journal of Non-Crystalline Solids*; 521: 119498. doi: 10.1016/j.jnoncrysol.2019.119498.
- [33]. Bezuidenhout, D. F. 1997. Calcium Fluoride (CaF₂). In: Palik, E. D. (ed.) *Handbook of Optical Constants of Solids*; Academic Press: Burlington, pp. 815-835.
- [34]. Zhan, J., Guo, Y., Wang, H. 2024. Electro-plastic effect on the indentation of calcium fluoride. *International Journal of Mechanical Sciences*; 261: 108693. doi: 10.1016/j.ijmecsci.2023.108693.
- [35]. Lee, H. W. 1926. The Hartmann formula for the dispersion of glass. *Transactions of the Optical Society*; 28(3): 161. doi: 10.1088/1475-4878/28/3/303.